

VARIABILITY OF TOTAL, BACK AND SIDE SCATTERING TO MASS CONCENTRATION OF MARINE PARTICLES

Griet Neukermans^{1,2}, Hubert Loisel², Xavier Mériaux², David McKee³, Rosa Astoreca⁴ and David Doxaran⁵

¹Management Unit of the North Sea Mathematical Models (MUMM), Brussels, Belgium

²ULCO, CNRS, UMR 8187, F-62930 Wimereux, France

³Department of Physics, University of Strathclyde, Glasgow, Scotland

⁴Laboratoire Ecologie des systèmes aquatiques (ESA), Université Libre de Bruxelles, Belgium

⁵Laboratoire d'Océanographie de Villefranche, Villefranche-sur-Mer, France

ABSTRACT

We investigate the relationship between various scattering properties (total, back and side scattering) and Total Suspended Matter (TSM), the dry mass concentration of marine particles in suspension, for coastal and offshore waters in various regions (Coastal Atlantic, Southern North Sea, Mediterranean Sea and French Guyana waters). We quantify the uncertainty on TSM concentration estimation from each scattering property. We further quantify the variability of the total (b_p), side (b_s) and back scattering (b_{bp}) to mass concentration ratio and explain this variability in terms of the physical (size) and chemical (apparent density, refractive index) properties of the particles. We show that b_{bp} , b_p and b_s correlate well with TSM (correlation coefficients higher than 0.92), though with considerable scatter along the regression line. We find that 75% of the predicted TSM concentrations from a model based on b_s are within 29% of the measured TSM concentration and within 38% and 48% for b_{bp} and b_p based models, respectively. The variability of mass specific total scattering (b_p^*) is mainly explained by total geometric cross section (PSA) and backscattering ratio (\tilde{b}_{bp}), with observations above (below) the regression line having significantly higher (lower) \tilde{b}_{bp} and lower (higher) PSA. Variability of mass specific backscattering (b_{bp}^*) was smaller and could not be explained by a single parameter. We do find that points below the regression line have significantly lower densities (ρ_a), PSA, refractive index (n), \tilde{b}_{bp} and chlorophyll a:TSM ratio than points near or above the line. After classification of observations in Case 1 and 2 water types, we find that Case 2 waters (N=149) show significantly higher values of b_{bp}^* , ρ_a , n , \tilde{b}_{bp} and PSA and significantly lower values for b_p^* and chl a:TSM than for Case 1 waters (N=123).

INTRODUCTION

The knowledge of mass specific inherent optical properties (IOP) is of fundamental importance for radiative transfer studies performed in natural waters, ocean color remote sensing applications, as well as for in situ monitoring of suspended marine particle dynamics. Following recent developments of

appropriate instrumentation for measurement of IOPs, studies were dedicated to the assessment of the relationships between particulate backscattering (b_{bp}) scattering (b_p), or attenuation (c_p) coefficients and total suspended matter concentration (TSM) (e.g. Babin *et al.*, 2003; Boss *et al.*, 2009; Bowers *et al.*, 2009; Martinez-Vicente *et al.*, 2010). The mass specific particulate scattering coefficient, b_p^* (b_p :TSM), is lower in Case 2 waters than in Case 1 waters, where IOPs are mainly driven by phytoplankton and associated material (Babin *et al.*, 2003). Bowers *et al.* (2009) show that the variability of b_p^* is mainly explained by changes in the apparent density (dry weight: wet volume). Based on in-situ experiments and theoretical modeling it was also shown that particle aggregation plays a major role in explaining the relatively narrow range of observations of the mass specific beam attenuation coefficient and its low sensitivity to particle size (Boss *et al.*, 2009). Based on a large in situ data set collected in different regions of the coastal and open ocean we re-investigate these relationships, with a specific focus on the mass specific particulate backscattering coefficient, b_{bp}^* (b_{bp} :TSM), for which the variability has still not been well characterized. We specifically examined the impact of particle size distribution, density, refractive index, trophic status, and Case 1/Case 2 classification.

MATERIALS AND METHODS

IN SITU MEASUREMENTS

Various sampling campaigns in coastal and offshore waters were conducted between April 2008 and July 2010. A total of 266 stations were visited: 213 in the Southern North Sea (April, June, July 2008, 09&10, September 2008&09, January 2010), 59 in the Coastal Atlantic (June 2008, 09&10), 60 in the Mediterranean Sea (March 2009) and 34 in French Guyana waters (October 2009). Sampling in the Southern North Sea covered the yearly blooms of *Phaeocystis globosa* and *Noctiluca scintillans*, and periods of lower biological activity as well.

Simultaneous measurements of IOPs, TSM and chlorophyll a, chl, were recorded at each station in surface waters. $b_p(\lambda)$ and $c_p(\lambda)$, were obtained from a WETLABS AC-9 or AC-S instrument at $\lambda=490, 510, 532, 600, 650, 676, 715, 765$ and 865nm . $b_{bp}(\lambda)$, was obtained from a WETLABS BB-9 instrument. An in situ Laser Scattering and Transmissometry device (LISST-100X, Sequoia Scientific Inc.) was used to obtain particle size distribution in the range $2\text{-}350\mu\text{m}$ (LISST type C), through inversion of the forward scattering signature for randomly shaped particles (Agrawal *et al.*, 2008).

TSM and chl concentration are obtained through on-board filtration of surface seawater (sampled with Niskin bottles) on triplicate and duplicate filters, respectively. The TSM median and interquartile range (IQR, difference between the 75th and 25th percentile value) were computed. Side scattering at 860nm at 90° was recorded with a portable turbidimeter HACH 2100P (compliant with the ISO7027 standard). Side scattering, b_s , expressed in units of FNU (Formazine Nephelometric Units) is recorded in triplicates before and after filtration, giving 6 replicates for which the median and IQR are computed. Variability of scattering and backscattering were quantified by the median and IQR values from a 5 minute surface deployment (giving about 300 records).

DERIVATION OF CHEMICAL AND PHYSICAL PROPERTIES OF MARINE PARTICLES

The LISST-100X (type C) provides the distribution of particle volume concentration C_{vi} (in $\mu\text{l/l}$) in 32 size classes logarithmically spaced within the range 2-350 μm , from which the particle size distribution (PSD) is derived. LISST data have been reported to show considerable instability in the smallest and biggest size range (*e.g.* Jouon *et al.*, 2008, Traykovski *et al.* 1999), which is likely due to the presence of particles smaller and coarser than the measured size range. Due to this instability, the outer and inner ring values were excluded when fitting the Junge power law distribution to the remaining data: $n(D_i) = KD_i^{-\gamma}$ with $2 \leq i \leq 31$, where $n(D_i)$ is the number of particles in size class i and γ is called the **Junge parameter**. Typical values of γ are 3-5. The number of particles and volume concentration in the extreme rings ($i=1,32$) were obtained through extrapolation of the Junge law to $n(D_1)$ and $n(D_{32})$, from which C_{v1} and C_{v32} are derived. The total volume concentration, VC ($\mu\text{l/l}$), is $VC = \sum_{i=1}^{32} C_{vi}$. The

apparent particle density, ρ_a , is the dry weight (TSM) to wet volume (VC) ratio. There is a size mismatch between these two quantities, as particles with a diameter $> 0.4\mu\text{m}$ are retained on a GF/F glass fibre filter (effective pore size of $0.7\mu\text{m}$), while the wet volume only accounts for particles in the 2-350 μm range. During bloom conditions in our dataset, strong deviations from the Junge law were observed leading to huge uncertainties on VC, when extrapolated to 0.7-1000 μm . For the sake of consistency, none of the PSD's was extrapolated further and the **apparent density, $\rho_a(\text{kg/l})$** is:

$$\rho_a = TSM : VC_{2\mu\text{m}}^{350\mu\text{m}} .$$

Total projected surface area, PSA (cm^2/l), which is thought to govern b_{bp} , more than TSM (Hatcher *et al.*, 2001), is calculated as follows: $PSA = \frac{3}{2} \sum_{i=1}^{32} 10 \frac{C_{vi}}{D_i}$

The **mean diameter**, weighed by area, D_A , is $D_A = \frac{\sum_{i=1}^{32} PSA_i \times D_i}{PSA}$.

The **backscattering ratio, \tilde{b}_{bp}** , represents the fraction of light scattered in the backward direction and reflects the biogeochemical composition (organic fraction, relative to phytoplankton) of the particles (Loisel *et al.*, 2007).

The particle **bulk refractive index, n** , was estimated from the **hyperbolic slope of the attenuation spectrum (χ)** and \tilde{b}_{bp} , following the Mie-theory based model of Twardowski *et al.* (2001): $n = 1 + \tilde{b}_{bp}^{(0.5377+0.4867\chi^2)} (1.4676 + 2.2950\chi^2 + 2.3113\chi^4)$. χ was calculated between 490 and 650nm and \tilde{b}_{bp} at 650nm.

DATA TREATMENT AND STATISTICAL ANALYSIS

b_{bp} , b_p and b_s were regressed against TSM concentration using a least squares approach in log log space. Observations were classified in three groups, based on 50% prediction bounds of the regression line: observations above (group G1), between (group G0) and below (group G-1) the 50% prediction bounds. The scatter from the log log regression line was examined by testing for significant differences in the chemical and physical properties (described previously) between these three groups. A Kruskal-Wallis test was performed, followed by a multiple comparison based on Tukey's least significant difference procedure to test for significant differences between groups.

Observations were classified in Case 1 and Case 2 waters according the relationship between $c_p(650\text{nm})$ and chl concentration established by Loisel and Morel (1998). This allowed a comparison of mass specific scattering coefficients and chemical/physical parameters described above between the two datasets. Since none of the parameters under investigation is normally or log-normally distributed, non-parametric Kruskal-Wallis tests were performed.

RESULTS AND DISCUSSION

RELATIONSHIP BETWEEN B_{BP} , B_p AND B_s AND TSM

The observed values of b_{bp} , b_p and b_s and TSM span about 4 orders of magnitude, as shown in Table 2. The number of observations classified as Case 1 or Case 2 are also tabulated.

Table 1. Total number of observations (N), classified as Case 1 or 2 (N Case 1, N Case 2), minimum, maximum and 25-50-75th percentile values of scattering properties and TSM.

Parameter	N	N case 1	N case 2	min	max	percentile values		
						25	50	75
TSM (mg/l)	366	123	149	0.1000	326.6667	0.6000	2.8000	14.0000
b_p (m^{-1})	308	100	126	0.0318	72.1859	0.4679	2.2389	7.1739
b_{bp} (m^{-1})	260	72	112	0.0016	0.3923	0.0049	0.0137	0.0931
b_s (m^{-1})	366	123	149	0.2150	488.0000	0.6200	3.2350	15.2500

TSM was regressed against b_{bp} , b_p and b_s in log log space. The regression equation (with 95% confidence bounds for the estimated coefficients), the number of observations (N) and the correlation coefficient (R^2) for b_{bp} , b_p and b_s are shown in Figures 1-3. The 50% prediction bounds of the regression are shown as dotted red lines. Correlations between the various scattering properties and TSM are high ($R^2 > 0.92$), with the back ($R^2 = 0.94$) and side ($R^2 = 0.97$) scattering methods being better predictors of TSM than total scattering.

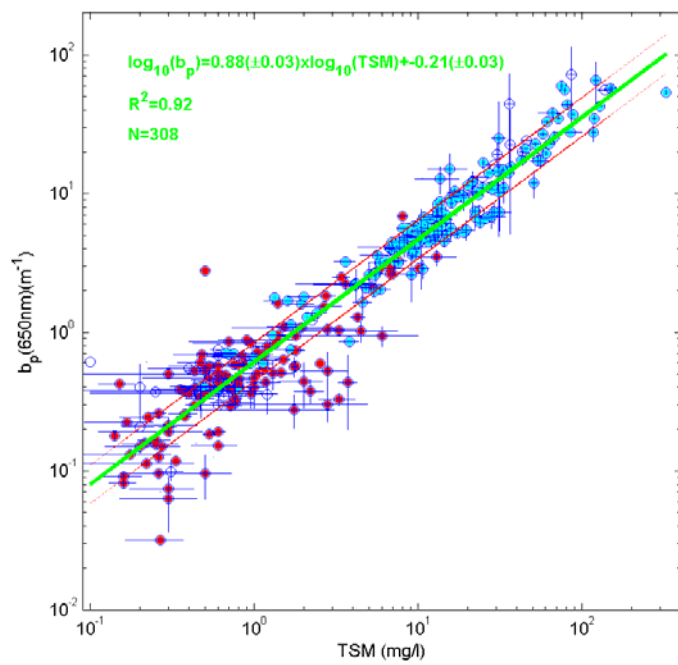


Figure 1. Log log regression between b_p (650nm) and TSM. Red for Case 1, blue for Case 2 waters. Error bars denote interquartile ranges.

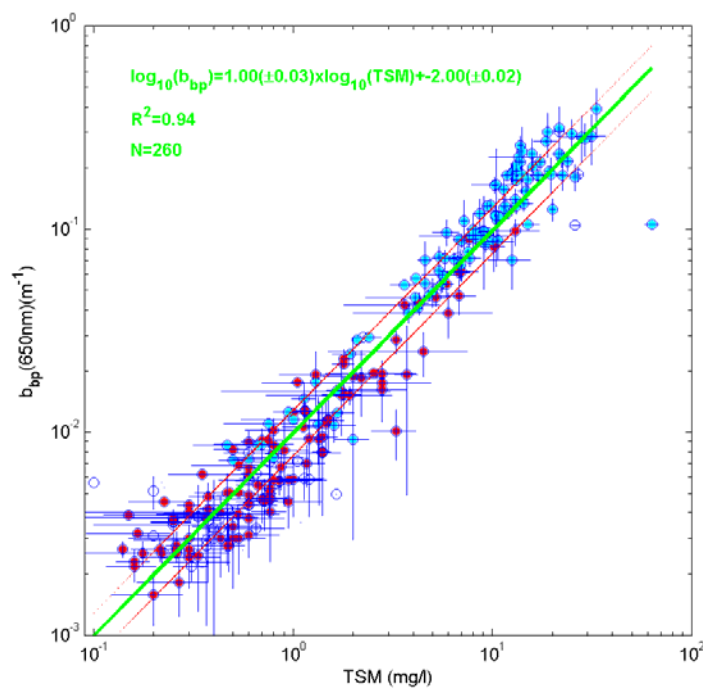


Figure 2. Log log regression between b_{bp} (650nm) and TSM. Red for Case 1, blue for Case 2 waters. Error bars denote interquartile ranges.

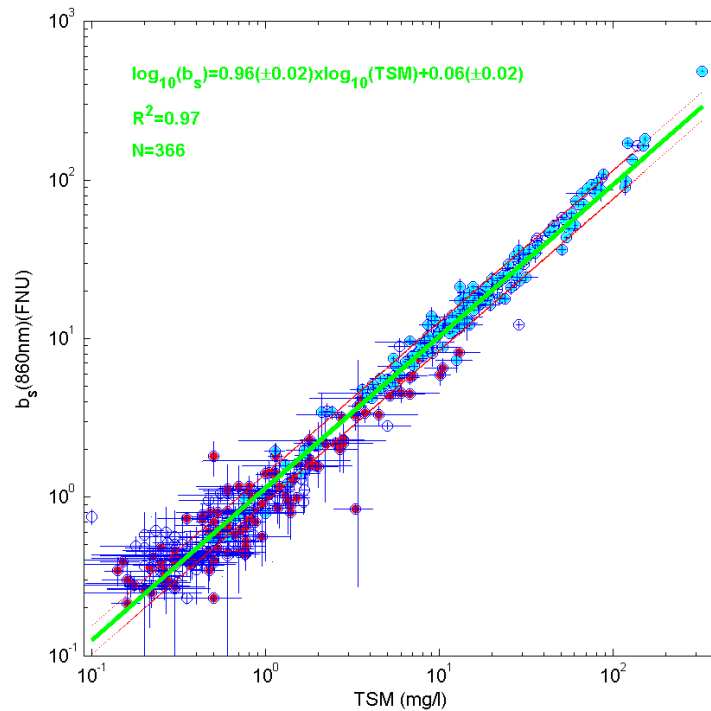


Figure 3. Log log regression between b_s and TSM. Red for Case 1, blue for Case 2 waters. Error bars denote interquartile ranges.

In analogy to the regression analysis in Figures 1-3, regression models to estimate TSM from a scattering property were derived. In order to quantify the error on the prediction of TSM concentration from a scattering property the percentage deviation of the regression model derived TSM to the observed TSM (*i.e.* $|\text{pred}_{\text{TSM}} - \text{obs}_{\text{TSM}}| : \text{obs}_{\text{TSM}}$) was computed. Only those stations where all three scattering properties were measured were retained (N=241). Table 3 gives the 5, 25, 50, 75 and 95 percentiles of these errors for TSM prediction from b_{bp} , b_{p} and b_{s} . For the b_{s} based regression model, we find that 50% of the model-predicted TSM concentrations are within 16% of the measured TSM concentration and 95% of the model-predicted TSM concentrations are within 62% of the observed TSM. The agreement is not as good for either b_{bp} or b_{p} . This might be because b_{s} was measured on the exact same water volume as the TSM concentration, while both b_{bp} and b_{p} were measured in-water. For comparison with Boss *et al.* (2009), we retained those observations in the TSM range 1.2 to 80mg/l (N=141), and the corresponding prediction percentile errors are given in brackets in Table 2. Boss *et al.* (2009) found overall better correspondence with median prediction errors for $c(660\text{nm})$ ($\approx b_{\text{p}}(650\text{nm})$) of 16%, $b_{\text{bp}}(700\text{nm})$ of 9% and $b_{\text{s}}(880\text{nm})$ of 21%.

Table 2. Prediction error: the ratio of the absolute value of the difference between a regression model derived TSM and its observed value to its observed value. Values between brackets for a model with $1.2 < TSM < 82.4 \text{ mg/l}$ (for comparison with Boss et al., 2009)

Pop. percentiles(%)	Prediction percentile error (%): model-TSM :TSM				
	5	25	50	75	95
bp	3 (2)	13 (11)	26 (22)	48 (40)	124 (77)
bbp	2 (2)	11 (7)	22 (19)	38 (33)	70 (49)
bs	1 (1)	7 (5)	16 (11)	29 (23)	62 (42)

EXPLAINING VARIABILITY IN B_p *

Kruskal-Wallis test results for significant differences between observations below (G-1), between (G0) and above (G1) the 50% prediction bounds of the log log regression line between b_p and TSM (shown in Figure 1) are given in Table 3. \tilde{b}_{bp} and PSA are the parameters with the most discriminatory power. G1 is characterized by significantly lower \tilde{b}_{bp} and higher PSA than G0 and G-1 has significantly higher \tilde{b}_{bp} and lower PSA than G0. G1 also has significantly lower n and D_A , with higher chl:a:TSM and γ and than the other two groups.

Table 3. Kruskal Wallis test results for significant differences between groups G0,G1 and G-1 from the b_p :TSM relationship (see text for details)

Parameter	N (-1,0,1)	p-value	G -1	G 0	G 1
ρ_a	57,139,34	>0.05			
n	57,139,34	4.3×10^{-6}	H than G1	H than G1	L than G0,-1
D_A	52,125,25	2.6×10^{-5}	H than G1	H than G1	L than G0,-1
bbp:bp	57,146,38	<tab	H than G0,1	L than G-1, H than G1	L than G0, -1
Chl:a:TSM	58,169,45	1.4×10^{-6}	L than G1	L than G1	H than G0,-1
PSA	52,125,25	1.6×10^{-6}	L than G0,1	L than G-1, H than G1	H than G0, -1
γ	52,127,28	1.1×10^{-4}	L than G1	L than G1	H than G0,-1

EXPLAINING VARIABILITY IN B_{BP} *

Overall, the scatter around the regression line is smaller than for b_p vs. TSM (see Figures 1-2). No single tested parameter showed significant differences between all three groups. We do find significantly lower ρ_a , n, PSA, and \tilde{b}_{bp} for G-1 than for G0 and G1.

Table 4. Kruskal Wallis test results for significant differences between groups G0,G1 and G-1 from the b_{bp} :TSM relationship (see text for details)

Parameter	N(-1,0,1)	p-value	G -1	G 0	G 1
ρ_a	41,81,34	2.3×10^{-6}	L than G0,1	H than G1,-1	L than G0
n	47,119,64	1.1×10^{-5}	L than G0,1	H than G-1	H than G-1
DA	45,85,36	0.06			
bbp:bp	56,121,64	1.5×10^{-7}	L than G0,1	H than G-1	H than G-1
Chla:TSM	55,127,56	1.1×10^{-4}	H than G0,1	L than G-1	L than G-1
PSA	45,85,36	7.2×10^{-5}	L than G0,1	H than G-1	H than G-1
γ	45,85,36	8.1×10^{-3}	L than G0	H than G-1	

CASE 1 - CASE 2 CLASSIFICATION

Case1-2 classification resulted in 123 Case 1 observations and 149 Case 2 observations. For the remaining 94 observations, no pigment data was available. For each parameter, the number of observations, the p-value (significance of the χ square statistic) of the test and the 25, 50 and 75 percentile values are given in Table 5. Results show significantly higher values of b_{bp}^* , ρ_a , n, \tilde{b}_{bp} and PSA for Case 2 waters and significantly lower values for b_p^* , γ_c and chla:TSM than for Case 1 waters. No significant differences were found for b_s^* , D_A and γ . The observed value of b_p^* for Case 2 waters is close to the value reported by Babin *et al.* (2003), *i.e.* ± 0.47 m²/g (from 0.51 at $\lambda=555$ nm, extrapolated to $\lambda=650$ nm). The value reported by Babin *et al.* (2003) for Case 1 waters (1 at $\lambda=555$ nm, 0.8 when extrapolated to $\lambda=650$ nm) is higher than the one we observe, which can be explained by the strong bloom conditions in the Case 1 waters included in this study.

Table 5. Overview of 25, 50 and 75 percentile values for Case 1 and Case 2 waters of mass specific IOPs and some selected physical and chemical properties. The p-value of the Kruskal-Wallis statistical tests and the number of observations is given. (<tab indicate p-values smaller than the tabulated value).

Parameter	Nobs	p-value	Case 1			Case 2		
			25	50	75	25	50	75
bp:TSM (m ² /g)	113,107	6.3×10^{-8}	0.3877	0.5929	0.7458	0.3835	0.4940	0.5782
bbp:TSM (m ² /g)	123,149	2.9×10^{-3}	0.0068	0.0088	0.0119	0.0099	0.0113	0.0137
bs:TSM (FNU l/mg)	123,149	>0.05	0.8192	1.0133	1.3233	0.9933	1.0871	1.1805
ρ_a (kg/l)	73,112	1.2×10^{-6}	0.0649	0.0879	0.1859	0.1336	0.2491	0.3439
bbp:bp	113,107	7.8×10^{-6}	0.0110	0.0169	0.0242	0.0178	0.0227	0.0309
n	113,107	4.9×10^{-12}	1.0836	1.1122	1.1522	1.1455	1.1731	1.2207
chla:TSM	123,149	<tab	0.0013	0.0019	0.0029	0.0001	0.0003	0.0006
PSA (cm ² /l)	67,105	<tab	2.3201	4.1235	11.7342	18.6078	32.7273	80.8637
DA (mum)	73,109	>0.05	24.4795	28.5084	40.4377	21.7227	30.5068	43.2055
γ	67,108	>0.05	3.2008	3.3975	3.5968	3.1975	3.4788	3.7350
γ (from χ)	111,142	6.6×10^{-10}	3.3699	3.7064	4.0195	3.3435	3.4828	3.6044

Bowers *et al.* (2009) report a mean apparent density of 0.264 kg/l along the South and West coast of Britain, with mainly mineral particles. The ρ_a we observe for Case 2 waters is close to this value (0.249kg/l). These apparent densities are much lower than the density of water because the particles, in an aggregated state, comprise water trapped within pieces of solid material and lose part of their mass when dried on a filter.

CONCLUSION

We show that b_{bp} , b_p and b_s correlate well with TSM (correlation coefficients higher than 0.92), though with considerable scatter along the regression line. We find that 75% of the predicted TSM concentrations from a model based on b_s are within 29% of the measured TSM concentration and within 38% and 48% for b_{bp} and b_p based models, respectively. The variability b_p^* is mainly explained by PSA and \tilde{b}_{bp} with observations above (below) the regression line having significantly higher (lower) \tilde{b}_{bp} and lower (higher) PSA. Variability of b_{bp}^* was smaller and could not be explained by a single parameter. We do find that points below the regression line have significantly lower ρ_a , PSA, n , \tilde{b}_{bp} and chl:TSM ratio than points near or above the line. After classification of observations in Case 1 and 2 water types, we find that Case 2 waters (N=149) show significantly higher values of b_{bp}^* , ρ_a , n , \tilde{b}_{bp} and PSA and significantly lower values for b_p^* and chl:TSM than for Case 1 waters (N=123).

ACKNOWLEDGEMENTS

This research was supported by the BELCOLOUR-2 project, funded by the STEREO programme of the Belgian Science Policy Office under contract SR/00/104. MUMM's Chemistry Laboratory is acknowledged for the analysis of TSM and chlorophyll data. The crew of the Belgica research vessel is thanked for their kind help during sea campaigns. The first author is involved in a MUMM-ULCO collaborative PhD research project. Her co-promoter, Kevin Ruddick, is thanked for his support.

REFERENCES

- Agrawal, Y.C., Whitmire A., Mikkelsen O.A. and H. C. Pottsmith, 2008. Light scattering by random shaped particles and consequences on measuring suspended sediments by laser diffraction. JOURNAL OF GEOPHYSICAL RESEARCH, 113, C04023.
- Babin M, Morel A, Fournier-Sicre V, Fell F, Stramski D, 2003. Light scattering properties of marine particles in coastal and open ocean waters as related to the particle mass concentration. LIMNOLOGY AND OCEANOGRAPHY, 48, 2, 843-859.
- Boss E, Taylor L, Gilbert S, *et al.*, 2009. Comparison of inherent optical properties as a surrogate for particulate matter concentration in coastal waters. LIMNOLOGY AND OCEANOGRAPHY-METHODS, 7, 803-810.
- Bowers DG, Braithwaite KM, Nimmo-Smith WAM, *et al.*, 2009. Light scattering by particles suspended in the sea: The role of particle size and density. CONTINENTAL SHELF RESEARCH, 29, 14, 1748-1755.
- Hatcher A, Hill P, Grant J, 2001. Optical backscatter of marine flocs. JOURNAL OF SEA RESEARCH, 46, 1, 1-12.

Jouon A, Ouillon S, Douillet P, *et al.*, 2008. Spatio-temporal variability in suspended particulate matter concentration and the role of aggregation on size distribution in a coral reef lagoon. *MARINE GEOLOGY*, 256, 1-4, 36-48.

Loisel H, Morel A, 1998. Light scattering and chlorophyll concentration in Case 1 waters: A reexamination. *LIMNOLOGY AND OCEANOGRAPHY*, 43,5,847-858.

Loisel H, Meriaux X, Berthon JF, *et al.*, 2007. Investigation of the optical backscattering to scattering ratio of marine particles in relation to their biogeochemical composition in the eastern English Channel and southern North Sea. *LIMNOLOGY AND OCEANOGRAPHY*, 52, 2,739-752.

Martinez-Vicente V, Land PE, Tilstone GH, *et al.*, 2010. Particulate scattering and backscattering related to water constituents and seasonal changes in the Western English Channel. *JOURNAL OF PLANKTON RESEARCH*, 32, 5, 603-619.

Traykovski P, Latter RJ, Irish JD, 1999. A laboratory evaluation of the laser in situ scattering and transmissometry instrument using natural sediments. *MARINE GEOLOGY*, 159, 1-4, 355-367.

Twardowski MS, Boss E, Macdonald JB, *et al.*, 2001. A model for estimating bulk refractive index from the optical backscattering ratio and the implications for understanding particle composition in case I and case II waters. *JOURNAL OF GEOPHYSICAL RESEARCH-OCEANS*, 106, C7, 14129-14142.